Inorganic Chemistry

pubs.acs.org/IC

Article

Cobalt Corroles as Electrocatalysts for Water Oxidation: Strong Effect of Substituents on Catalytic Activity

Nicolás I. Neuman,* Uta Albold, Eleonora Ferretti, Shubhadeep Chandra, Simon Steinhauer, Paul Rößner, Franc Meyer, Fabio Doctorovich, Santiago E. Vaillard, and Biprajit Sarkar*

Cite This: https://dx.doi.org/10.1021/acs.inorgchem.0c02550

Read Online

ACCESS | Metrics & More | Article Recommendations | Supporting Information

ABSTRACT: Two Co(III) complexes ($\mathbf{1Py_2}$ and $\mathbf{2Py_2}$) of new corrole ligands $\mathbf{H_3L1}$ (5,15-bis(*p*-methylcarboxyphenyl)-10-(*o*-methylcarboxyphenyl)corrole) and $\mathbf{H_3L2}$ (5,15-bis(*p*-nitrophenyl)-10-(*o*-methylcarboxyphenyl)corrole) with two apical pyridine ligands have been synthesized and thoroughly characterized by cyclic voltammetry, UV−vis−NIR, and EPR spectroscopy, spectroelectrochemistry, single-crystal X-ray diffraction studies, and DFT methods. Complexes $\mathbf{1Py_2}$ and $\mathbf{2Py_2}$ possess much lower oxidation potentials than cobalt(III)-*tris*-pentafluorophenylcorrole (Co(tpfc)) and similar corroles containing pentafluorophenyl (C_6F_5) substituents, thus allowing access to high oxidation states of the former metallocorroles using mild chemical oxidants. The spectroscopic (UV−vis−NIR and EPR) and electronic properties of several oxidation states of these complexes have been determined by a combination of the mentioned methods. Complexes $\mathbf{1Py_2}$ and $\mathbf{2Py_2}$ undergo three oxidations within 1.3 V vs FcH^+/FcH in MeCN, and we show that both complexes catalyze water oxidation in an MeCN/H_2O mixture upon the third oxidation, with k_{obs} (TOF) values of 1.86 s^{-1} at 1.29 V ($\mathbf{1Py_2}$) and 1.67 s^{-1} at 1.37 V ($\mathbf{2Py_2}$). These values are five times higher than previously reported TOF values for C_6F_5-substituted cobalt(III) corroles, a finding we ascribe to the additional charge in the corrole macrocycle due to the increased oxidation state. This work opens up new possibilities in the study of metallocorrole water oxidation catalysts, particularly by allowing spectroscopic probing of high-oxidation states and showing strong substituent-effects on catalytic activity of the corrole complexes.

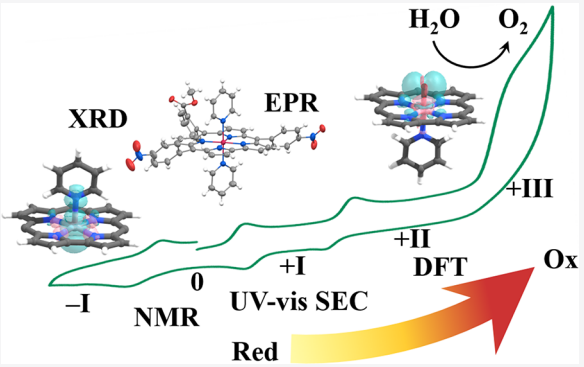

1. INTRODUCTION

The interest in corroles has continuously increased in the past 20 years because of their rich chemical, catalytic, photophysical and spectroscopic properties.[1−4] The corrole macrocycle has three dissociable protons and thus usually acts as a trianionic ligand for metals ions,[1,2] stabilizing higher formal metal oxidation states and destabilizing lower oxidation states. Because of this, the overpotential for certain oxidation reactions may be reduced while the kinetic rate of reduction reactions may be increased.[5] Corrole metal complexes have been shown to catalyze reactions of synthetic value such as hydroxylation, epoxidation, or cyclopropanation.[1,6] They have also been used in energy conversion reactions such as proton,[7−9] oxygen,[10,11] or carbon dioxide reduction,[5,12] as well as water oxidation.[13,14]

Water oxidation (WO) to dioxygen is possibly the most environmentally benign reaction that can be coupled to H_2 production or CO_2 reduction to generate green fuels,[15] and many homogeneous molecular[16,17] and heterogeneous[18] water oxidation catalysts (WOCs) have been and are continuously being studied. Although heterogeneous WOCs are usually considered to be more robust, especially in the case of metal oxides,[19] molecular catalysts usually allow access to mechanistic information through spectroscopic and electrochemical methods. Furthermore, the properties of molecular catalysts can be more easily tuned through synthetic means, in principle allowing a systematic improvement of the catalyst properties.

Water oxidation catalyzed by metallocorroles is usually considered to occur through a rate-determining step involving water nucleophilic attack (WNA) on an oxidized metal-oxo species,[13,14,20] giving rise to an O−O bond. Some of the most commonly studied metallocorroles in water oxidation electrocatalysis, possess *meso*-pentafluorophenyl (C_6F_5) substituents, as for example Co(tpfc)[21] and Co"Hangman" corrole,[13] (Scheme 1). The ability of Co(tpfc) as a water oxidation catalyst has been extensively studied,[10,11] as well as the role of different apical ligands, such as substituted pyridines,[22] or

Received: August 26, 2020

Scheme 1. Chemical Structures of Selected Cobalt Corrole Water Oxidation Catalysts with C_6F_5 Substituents

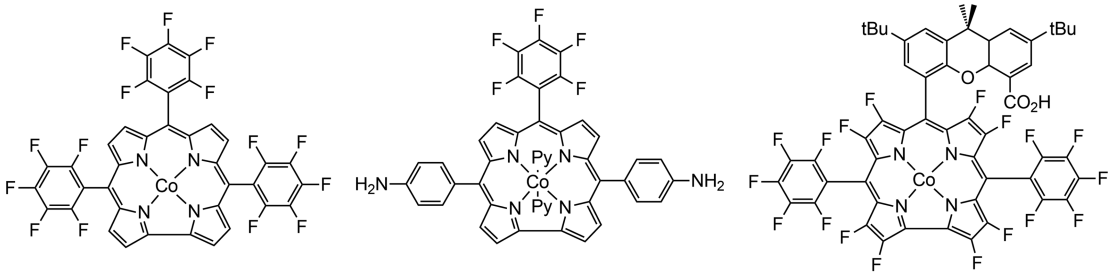

fluoride and hydroxide anions,[23] on its redox characteristics and catalytic performance. More recently, a cobalt corrole with aminophenyl and pentafluorophenyl substituents (Co(BAPC)-Py_2, Scheme 1) has also been shown to be an H_2O oxidation catalyst.[24]

The popularity of C_6F_5-containing corroles in electrocatalysis is partly due to historic reasons, as tris(pentafluorophenyl)corrole (tpfc), together with triphenylcorrole (tpc), was one of the first corroles synthesized by facile methods from pyrrole and aldehydes.[25,26] Probably the main reason for the many studies involving corroles with C_6F_5 substituents is the increased stability that these highly electron-withdrawing groups confer on the corrole macrocycle. Compared to other phenyl-substituted corroles, the electron-withdrawing characteristics of C_6F_5-substituted corroles lead to the formation of metal complexes that are relatively easy to reduce and hard to oxidize. Metallocorroles with substituents that are less electron-withdrawing than the C_6F_5 group and that therefore require lower potentials to reach the catalytically active high oxidation states could show improved catalytic performance. In the pursuit of better catalysts, it is also necessary to be able to systematically modify the catalyst's steric, electronic, and acid/base properties by changing the ligand substituents. In this respect, the C_6F_5 substituents are somewhat limited, as they usually can be functionalized only in the distant para-position through nucleophilic aromatic substitution.[5,25] On the other hand, methylester or nitro groups are versatile substituents that are moderately or strongly electron-withdrawing but that can also be converted by facile methods to mildly electron-donating carboxylate or strongly electron-donating (dialkyl)amino groups. Carboxylate and amino groups can also act as acid/base groups near the catalytic site, as has been shown in the case of "Hangman" corroles,[13] or can increase water solubility. Metallocorroles with less-electron-withdrawing groups have been thoroughly studied by spectroscopic, electrochemical, and computational methods,[3,4,27] and many of these have been explored as catalysts for O_2 reduction.[28] However, there have been few studies focusing on metallocorrole water oxidation catalysts without C_6F_5 groups. These were mostly performed with Mn metallocorroles,[14,20,29] and to the best of our knowledge no Co metallocorroles without C_6F_5 groups have been reported to perform water oxidation.[30]

In this work, we have focused on the synthesis and characterization of cobalt corroles that contain either *p*-methylcarboxyphenyl (**1**) or *p*-nitrophenyl (**2**) and *o*-methylcarboxyphenyl (**1** and **2**) *meso*-substituents. These compounds are meant to provide reference data for subsequent studies in which the *o*-methylcarboxyphenyl group is hydrolyzed to provide a proton shuttling carboxylate near the active site. The structural formulas of the cobalt(III) corroles studied in this work are shown in Scheme 2. We provide a thorough analysis of the complexes' spectroscopic properties in solution and by combining spectroscopic and electrochemical techniques with systematic density functional theory studies we focus on the investigation of the one- and two-electron oxidized products. Using cyclic voltammetry we also show that these metallocorroles are active water oxidation catalysts and discuss their differences with previously reported C_6F_5-containing cobalt corrole WOCs. We show that although the latter have been shown to perform water oxidation upon their second oxidation, the cobalt corroles studied in this work are able to catalyze this reaction when oxidized three times. This work provides a point of comparison for further studies on the carboxylate forms of these and similar cobalt corroles.

Scheme 2. Cobalt(III) Bis(pyridine) Corrole Complexes Synthesized and Studied in This Work

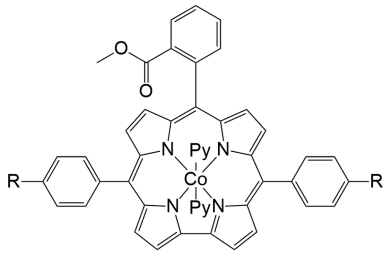

2. RESULTS AND DISCUSSION

Synthesis. Corroles H_3**L1** and H_3**L2** could be obtained in large scale (1 g and 500 mg, respectively) and moderate yields by using the method pioneered by Koszarna and Gryko.[31] H_3**L1** and H_3**L2** were characterized by ^{1}H NMR and UV−vis spectroscopy, elemental analysis, and mass spectrometry. Details on the synthesis, characterization, and analytical data are given in the Supporting Information. Crystallization attempts from DCM/hexane produced microcrystalline powders.

Cobalt Complexes of Corroles. The Co(III) complexes of corroles H_3**L1** (**Co(III)L1Py$_2$** or **1Py$_2$**) and H_3**L2** (**Co(III)L2Py$_2$** or **2Py$_2$**), which also bear two apical pyridine ligands, were obtained by adding a solution of the cobalt salt ($Co(Ac)_2{\cdot}4H_2O$) in MeOH to the free-base corroles in a mixture of pyridine and DCM, with O_2 likely acting as oxidant.

https://dx.doi.org/10.1021/acs.inorgchem.0c02550
Inorg. Chem. XXXX, XXX, XXX−XXX

The color change was immediate, although subtle; the blue-green color of H_3L1 lost its blue tinge, whereas for H_3L2, the color became brown-green. The solutions of metalated corroles were filtered through a large funnel that was equipped with silica, eluting with DCM that contained small amounts of pyridine. The solvent was removed under reduced pressure until a concentrated pyridine solution of the product was obtained. DCM was added again and the mixture subsequently layered with *n*-hexane. Applying this method, a large amount of crystals could be obtained, which were collected and washed with pentane. $1Py_2$ and $2Py_2$ were characterized by ^{1}H NMR spectroscopy, elemental analysis, mass spectrometry, cyclic voltammetry, and UV−vis−NIR spectroelectrochemistry, as well as chemical oxidation and reduction followed by UV−vis−NIR and EPR spectroscopy. DFT calculations were used to rationalize and complement the experimental observations.

X-ray Crystallography. X-ray diffraction quality single crystals of $2Py_2$ (Figure 1) were obtained by vapor diffusion of hexane into a concentrated DCM solution of the cobalt corrole with a few drops of added pyridine. The crystals grew as aggregated dark purple blocks of rhombic shape.

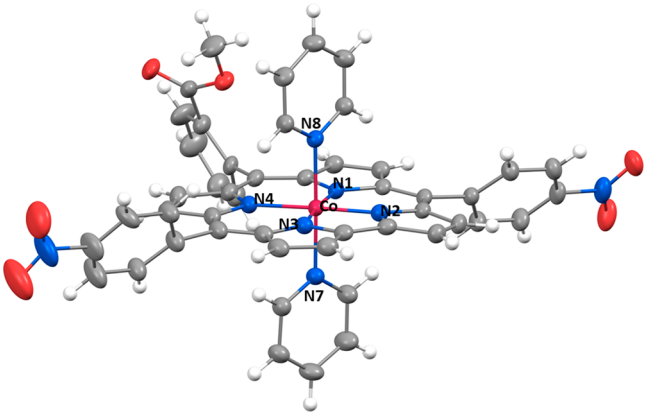

Figure 1. ORTEP representation of $2Py_2$. Ellipsoids are drawn at the 50% probability level, disorder in the 2-methylcarboxyphenyl, and one of the 4-nitrophenyl substituents are omitted for clarity (see Figure S22). Gray, C; blue, N; red, O; white, H; fuchsia, Co.

Compound $2Py_2$ crystallizes in the orthorhombic space group *Pbcn*, with eight molecules per unit cell and one molecule in the asymmetric unit. The cobalt is coordinated in a distorted octahedral environment with axial elongation of the Co−N bonds to the pyridine molecules. The Co−N distances lie in the range of reported bond distances for corrole complexes with low-spin Co(III) centers[32] (Table 1, **Co[TpMePC]Py$_2$**, **(Me$_4$Ph$_5$Cor)Co(py)$_2$**[33] and (5,15-bis(mesityl)-10-(p-F,m-NO$_2$Ph)cor)Co(Py)$_2$[28]). Crystallographic information is given in Tables S2 and S3, and in Table S4, the experimentally determined bond distances are compared to the distances obtained from DFT optimizations of $2Py_2$.

Cyclic Voltammetry. To elucidate the electrochemical properties of $1Py_2$ and $2Py_2$, we performed cyclic voltammetry measurements. $1Py_2$ displays two reversible oxidations at −0.21 and 0.53 V in CH_2Cl_2/0.1 M Bu_4NPF_6 (Figure 2, top, all potentials are reported vs the FcH$^+$/FcH couple), one quasi-reversible reduction at −0.77 V, and an irreversible reduction at −2.06 V. On the basis of our EPR spectroscopic measurements, DFT calculations, and previously reported studies,[4,23] we assigned the first and second oxidations to corrole centered processes and the first reduction to the Co(III)/Co(II) redox couple. The quasi-reversibility of the latter process is due to the dissociation equilibrium of one apical pyridine ligand, which has been extensively studied by Kadish et al.[34,35] Upon an increase in the scan rate (Figures S23 and S24), the first reduction becomes more irreversible,

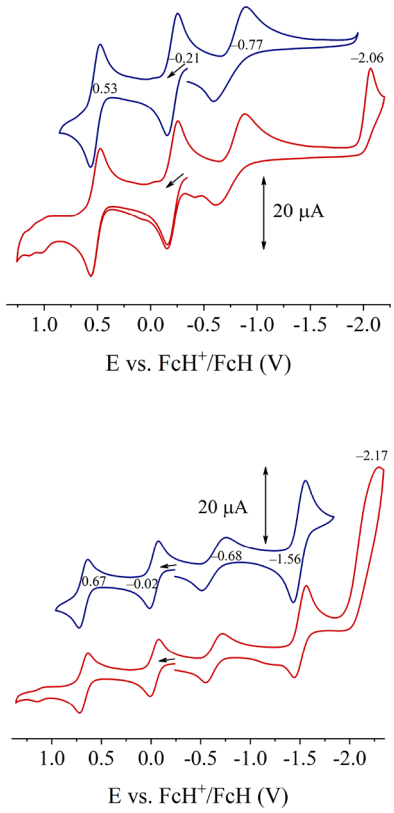

Figure 2. Cyclic voltammetry of $1Py_2$ (0.98 mM) (top) and $2Py_2$ (0.86 mM) (bottom) in 0.1 M Bu_4NPF_6 in DCM, at 50 mV/s.

Table 1. Cobalt−Nitrogen Bond Distances of $2Py_2$ in Å, Obtained from Single-Crystal X-ray Diffraction Analysis[a]

bond	$2Py_2$	bond	Co[TpMePC]Py$_2$[32]	bond	Me$_4$Ph$_5$CorCo(py)$_2$	bond	1[b]
Co−N1	1.897(2)	Co1−N3	1.902(2)	Co−N21	1.886(6)	Co1−N1	1.8718(17)
Co−N2	1.905(2)	Co1−N2	1.901(2)	Co−N22	1.915(6)	Co1−N2	1.8679(17)
Co−N3	1.871(2)	Co1−N1	1.868(2)	Co−N23	1.892(6)	Co1−N3	1.8996(17)
Co−N4	1.875(2)	Co1−N4	1.869(2)	Co−N24	1.884(5)	Co1−N4	1.8960(16)
Co−N7	1.993(2)	Co1−N100	1.994(2)	Co−N59	1.980(7)	Co1−N5	1.9822(17)
Co−N8	1.998(2)	Co1−N200	1.987(2)	Co−N65	2.003(7)	Co1−N6	1.9972(17)

[a]Selected bond distances for literature-known low-spin Co(III) corrole complexes with apical pyridine ligands are given for comparison. [b](5,15-Bis(mesityl)-10-(p-F,m-NO$_2$Ph)cor)Co(Py)$_2$.[28]

https://dx.doi.org/10.1021/acs.inorgchem.0c02550
Inorg. Chem. XXXX, XXX, XXX−XXX

Table 2. Half-Wave and Cathodic Peak Potentials of Complexes $1Py_2$ and $2Py_2$ and Two Literature Known Cobalt Corroles for Comparison in V

	solvent	E_p (Ox3)	$E^{0\prime}$ (Ox2)	$E^{0\prime}$ (Ox1)	$E^{0\prime}$ (Red1)	$E^{0\prime}$ (Red2)	E_p (Red3)
$1Py_2$	DCM		0.53	−0.21	−0.77	−2.06	
$2Py_2$	DCM		0.67	−0.02	−0.68	−1.56	−2.17[a]
$1Py_2$	MeCN	1.26[a]	0.30	−0.31	−0.80	−2.14	
$2Py_2$	MeCN	1.33[a]	0.40	−0.20	−0.75	−1.69	
Co(tpfc)[14,38]	MeCN		0.94	0.35	−0.36		
Co[TpXC](Py)$_2$[32b]	DCM		0.38-0.55	−0.29-(−0.13)	−0.83-(−0.75)	−2.25-(−2.10)	
			Ox4	Ox3	Ox2	Ox1	Red1
(Me_4Ph_5Cor)Co[33]		DCM	0.785	0.395	0.145	−0.025	−0.625
(Me_4Ph(p-OMePh)$_4$Cor)Co[33]		DCM	0.675	0.395	0.075	−0.095	−0.655

[a]Peak potential for irreversible processes. [b]The reported potentials, originally referenced to SCE, were rereferenced to FcH^+/FcH (475 mV vs SCE in DCM)[39] for comparison purposes. The values in the table indicate the range of potentials for the pX = *p*-CF_3, *p*-H, *p*-Me, and *p*-OMe series.

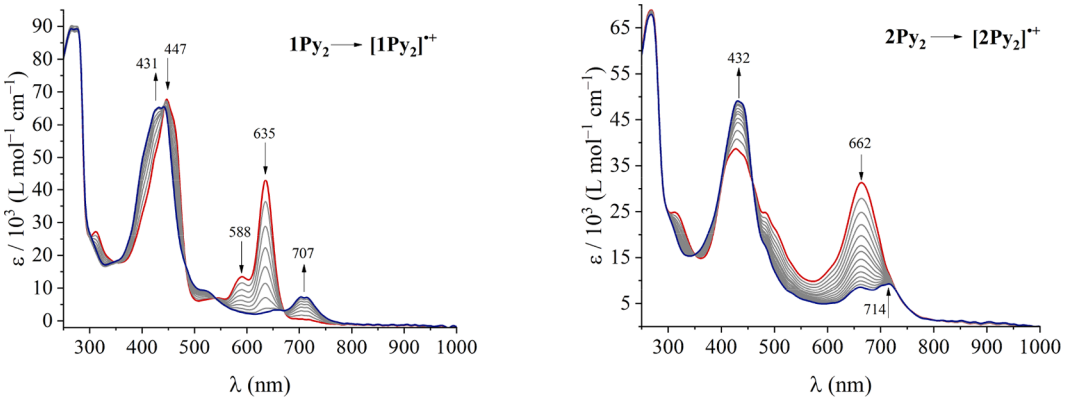

Figure 3. Change in the UV−vis−NIR absorption of $1Py_2$ (left) and $2Py_2$ (right) during the first oxidation in a DCM/pyridine mixture, Bu_4NPF_6 as supporting electrolyte. The reaction arrows indicate oxidation.

and the reoxidation wave shifts to more positive potentials. This suggests that reassociation of Py is relatively slow, and at fast scan rates, the reoxidation wave at −0.42 V corresponds to the $1Py^-$ to **1Py** oxidation. Dissociation of pyridine is further supported by the fact that when O_2 is allowed in the cell there is a catalytic current at −1.5 V compatible with cobalt corrole-catalyzed O_2 reduction (see Figure S28). For O_2 to bind to the Co(II) center, prior dissociation of one Py ligand is necessary.

If the potential is scanned beyond the irreversible wave at −2.06 V, corresponding to the formal Co(II)/Co(I) reduction, a series of reoxidation waves appear next to the normal redox processes of $1Py_2$. Highly reduced cobalt centers are known to react with CH_2Cl_2 and other alkyl halides,[36,37] so these waves could correspond to reoxidation of a byproduct of the reaction of $[1Py]^2$ and CH_2Cl_2. When the potential was scanned until −1.4 V, no secondary reoxidation waves appeared. This set of reoxidation waves does not appear at low scan rates (10 mV/s or 25 mV/s), but it starts to become more prominent when the scan rate is increased. This byproduct does not seem to accumulate over several scans, either at low or high scan rates, and seems to revert to $1Py_2$ after the second oxidation. The quasireversibility of the first reduction is completely independent of the irreversibility of the second reduction, which is completely irreversible at least until 2 V/s scan rate (see Figure S24). We also performed cyclic voltammetry studies of $1Py_2$ in MeCN/0.1 M Bu_4NPF_6 (see Figure S29), in which case the CV responses are similar to those in DCM, except that the second reduction, at −2.14 V, is now quasi-reversible, and a third irreversible oxidation is observed at 1.26 V (peak potential).

The cyclic voltammograms of $2Py_2$ in DCM (Figure 2, bottom) and MeCN (Figure S29) are similar to those of $1Py_2$. The redox potentials of $2Py_2$ in DCM and MeCN are, however, anodically shifted compared to the potentials of complex $1Py_2$, due to the *p*-nitrophenyl substituents of $2Py_2$, which themselves each undergo a one-electron reversible reduction at −1.50 V and an irreversible reduction at −2.16 V in DCM. This has been observed for nitrophenyl containing corroles before.[28] The first quasireversible reduction of $2Py_2$, which as in the case of $1Py_2$ corresponds to the Co(III)/Co(II) redox couple, occurs at −0.68 V in DCM and −0.75 V in MeCN. The first reversible oxidation, which is ligand centered, occurs at −0.02 V in DCM and −0.20 V in MeCN. The second oxidation is reversible in DCM (0.67 V) and quasi-reversible in MeCN (0.40 V). In MeCN a third irreversible oxidation can be observed at 1.33 V (peak potential). The reversibility of the second oxidation of $1Py_2$ and $2Py_2$ in DCM and the quasireversibility in MeCN hint at a possible replacement of pyridine (Py) by the latter solvent.

The redox potentials of $1Py_2$ and $2Py_2$ are shown in Table 2, together with the redox potentials of literature-known cobalt corroles with strong electron-withdrawing substituents (Co(tpfc)) or substituents of varying electron-donating or -withdrawing characteristics. In general, the redox processes of $1Py_2$ and $2Py_2$ are observed at 200−400 mV more negative potentials than the ones observed for Co(tpfc),[14,38] and they lie in a similar range to the redox potentials of reported Co[TpXC]Py_2 corroles (TpXC = 5,10,15-*tris*(pX-phenyl)-corrole; pX = *p*-CF_3, *p*-H, *p*-Me, and *p*-OMe substituents).[32] On the other hand, cobalt corroles with alkyl and aryl

https://dx.doi.org/10.1021/acs.inorgchem.0c02550
Inorg. Chem. XXXX, XXX, XXX−XXX

substituents in β-positions are much easier to oxidize than the meso-substituted corroles here described. This is to be expected given the electron-donating effect of the alkyl substituents. The effect of phenyl substituents on the β-positions is probably overall donating when the charge on the corrole macrocycle becomes positive. Table 2 shows two examples of such cobalt corroles reported by Kadish et al.[33]

UV−vis−NIR Spectroelectrochemistry and Chemical Oxidation. We performed UV−vis−NIR spectroelectrochemical measurements on complexes **1Py$_2$** and **2Py$_2$** in DCM, using an OTTLE cell.[40] We added a drop of pyridine to the DCM solutions to shift the equilibrium fully to the hexacoordinated species in order to facilitate interpretation. The changes in the UV−vis spectra of **1Py$_2$** and **2Py$_2$** during the first oxidation at 0.5 V vs Ag pseudoreference electrode are shown in Figure 3. The Soret band of **1Py$_2$** is blue-shifted from 447 to 431 nm, whereas for **2Py$_2$**, it is red-shifted from 426 to 433 nm. Additionally, the strong Q-bands of **1Py$_2$** (635 nm) and **2Py$_2$** (665 nm) form new maxima with less intensity at 707 and 715 nm, respectively. These changes were shown to be reversible. The disappearance of the strong Q-band suggests that the first oxidation may be located at the corrole macrocycle, whereas the added pyridine (absorption at 275 nm) renders dissociation of one of the axial pyridine ligands very unlikely.

Given that by cyclic voltammetry the potential of the first oxidation of both complexes was found to be negative with respect to ferrocene, we decided to also perform chemical oxidation using $[Fe(Cp)_2]PF_6$ in DCM. The changes in the UV−vis spectra are shown in Figure 4.

At the applied concentration (approximately 15 μM), the cobalt corroles were dissolved in their pentacoordinated state, which can be clearly seen by their native spectra (compare Figure 4 to Figures S20 and S21). The oxidation of **1Py** with $[Fe(Cp)_2]PF_6$ caused a shift of the Soret band from 393 to 435 nm and of the Q-band from 563 to 707 nm. For **2Py** the Soret band shifted from 378 to 433 nm and the Q-band from 572 to 713 nm. The final spectra of the chemically oxidized complexes are very similar to those generated by SEC measurements with excess pyridine. These results show that when oxidized, the pentacoordinated, neutral species **Co(III)LPy** increases its affinity for pyridine and forms an oxidized $[\mathbf{Co(III)LPy_2}]^{\bullet+}$.

EPR Spectroscopy. To gain further insights into the electronic structure of the different oxidation states of **1Py$_2$** and **2Py$_2$**, we combined chemical reduction or oxidation of these complexes with EPR spectroscopy. EPR spectra of reduced **1Py$_2$** (**Co(III)L1Py$_2$**) and **2Py$_2$** (**Co(III)L2Py$_2$**) were acquired by adding an excess of $Co(Cp)_2$ (−1.33 V vs FcH^+/FcH) to the DCM or THF solution of the respective cobalt corroles. At temperatures below 220 K, an anisotropic EPR signal appeared, which became better resolved below 150 K. Figure 5 shows the EPR signals observed at 100 K for both cobalt corroles, together with spectra simulated using the *EasySpin* package.[41] The EPR parameters derived from least-squares fitting the simulations to the experimental spectra are shown in Table 3. The Montecarlo and Simplex algorithms as implemented in *EasySpin* were used in the fittings. These signals are typical of low-spin Co(II) species (S = 1/2),[42] and indicate a metal centered reduction. Therefore, we assigned these signals to the pentacoordinated $[\mathbf{Co(II)L1Py}]^-$ and $[\mathbf{Co(II)L2Py}]^-$ forms. Dissociation of one of the pyridine ligands is supported by the observation of three well-resolved peaks in the g_z region of $[\mathbf{Co(II)L2Py}]^-$, which arise from

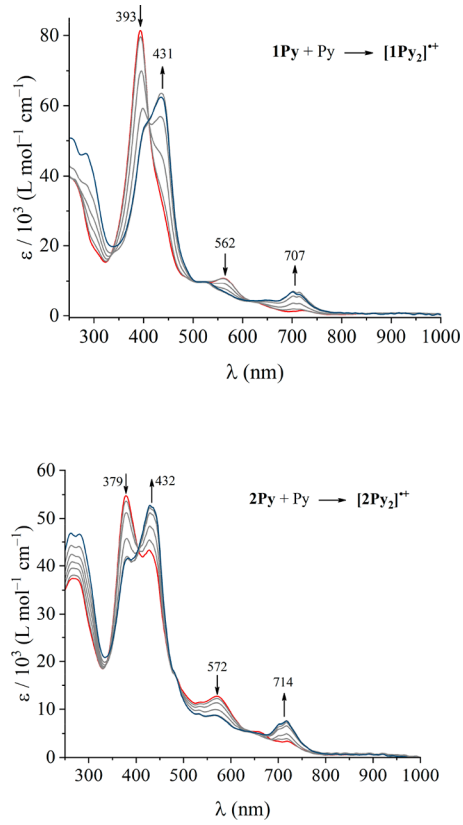

Figure 4. Changes in the UV−vis−NIR spectra upon the addition of increasing amounts of $[Fe(Cp)_2]PF_6$ to a DCM solution of **1Py** + Py (top), and **2Py** + Py (bottom). The reaction arrows indicate oxidation.

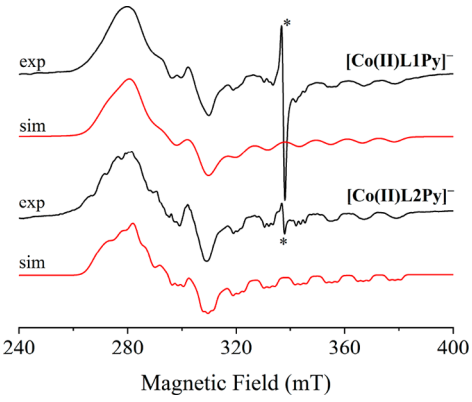

Figure 5. Experimental (black) and simulated (red) EPR spectra of $[\mathbf{Co(II)L1Py}]^-$ (top, DCM) and $[\mathbf{Co(II)L2Py}]^-$ (bottom, THF), generated by the reduction of the neutral corroles using $Co(Cp)_2$. The asterisk marks an as yet unidentified radical. Spectra were acquired at 100 K.

superhyperfine coupling of the metal-centered spin with an apical ^{14}N nucleus (I = 1).[43] No superhyperfine splitting to the corrole N nuclei was observed. Simulation of the signals allowed the determination of the anisotropic g and A values, both of which present rhombic symmetry. For both complexes, the EPR spectra showed a radical signal with g = 2.002, which we cannot at this point identify; this signal was more intense in the case of reduced **1Py$_2$** and is clearly distinguishable from the **Co(III)L1PyO$_2$**$^{\bullet-}$ (cobalt(III)-superoxido) signal,[23,44] which could be easily obtained by performing reduction of **1Py$_2$** with

https://dx.doi.org/10.1021/acs.inorgchem.0c02550
Inorg. Chem. XXXX, XXX, XXX−XXX

Table 3. *g* Values, Hyperfine *A* Values (MHz), and Isotropic and Anisotropic Linewidth Contributions Obtained by Least-Squares Fitting of Simulated EPR Spectra to the Experimental Spectra

	$[Co(II)L1Py]^-$	$[Co(II)L2Py]^-$		$[Co(III)L1Py_2]^{\bullet+}$	$[Co(III)L2Py_2]^{\bullet+}$
$g_{x,y,z}$	2.340, 2.287, 2.000	2.374, 2.276, 1.998	g_{iso}	2.0023	2.0022
$A_{x,y,z}$ (Co) (MHz)	160, 92.5, 322	159.7, 98.4, 320.4	A_{iso} (Co)	16.45	16.33
$A_{x,y,z}$ (N) (MHz)		n.d., n.d., 60			
lwpp[a] (mT)	4.59, 1	1.79, 1	lwpp (mT)	0.88, 0.095	0.86, 0.15
$HStrain_{x,y,z}$(MHz)	207, 150, 0	104, 120, 0			
solvent	DCM	THF		DCM	DCM
temperature	100 K	100 K		278 K	278 K

[a]The first value corresponds to Gaussian and the second to Lorentzian shape.

$Co(Cp)_2$ in O_2-saturated DCM solution. Both signals are shown in Figure S30. The radical signal observed for reduced $\mathbf{1Py_2}$ is also different from the radical signal obtained from the oxidation of $\mathbf{1Py_2}$, which will be discussed in the following paragraphs.

The hexacoordinated compounds $\mathbf{1Py_2}$ and $\mathbf{2Py_2}$ showed no EPR signal neither at 5 °C nor −170 °C in DCM (Figure 6, top and Figure S31). When $[Fe(Cp)_2]PF_6$ (0 V by definition) was added to the cobalt corrole solutions the color immediately changed from green to brown, and a strong EPR signal appeared (Figure 6 and Figure S31). This signal is isotropic and centered on a *g* value of 2.0023, with a pattern that indicates some type of unresolved hyperfine splitting. Very accurate simulations of these signals were obtained by considering an $S = 1/2$ system with hyperfine coupling to the ^{59}Co nucleus ($I = 7/2$). No ^{14}N hyperfine couplings have been resolved. The simulation parameters are listed in Table 3. These results clearly point to a corrole centered radical with small hyperfine coupling to the cobalt nucleus. We note that a different interpretation was given for very similar signals obtained in other cobalt corroles in ref 32. These findings are in complete agreement with the spin populations of the first oxidation products, calculated by DFT (see Table S5).

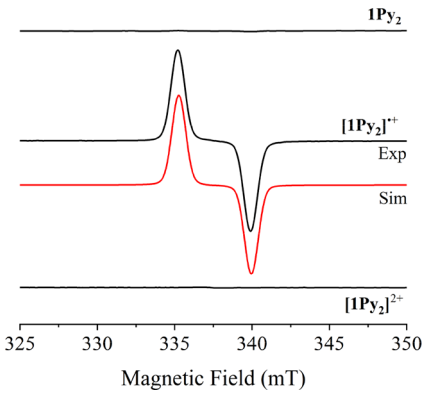

Figure 6. EPR spectra of native $\mathbf{1Py_2}$ (top), of the singly oxidized product $[\mathbf{1Py_2}]^{\bullet+}$ (center, black), together with its simulation (red) and of the two-times oxidized product, described for simplicity as $[\mathbf{1Py_2}]^{2+}$ (bottom, no signal). Spectra were acquired in DCM at 278 K.

When solid $AgPF_6$ ($EAg^+/Ag^0 = 0.65$ V vs FcH^+/FcH in DCM)[45] was added to the DCM solutions of $[\mathbf{1Py_2}]^{\bullet+}$ or $[\mathbf{2Py_2}]^{\bullet+}$, the color changed from brown to bright red, and the EPR signals disappeared (Figure 6, bottom and Figure S31, bottom). UV−vis spectra of the oxidized species were recorded and are shown in Figure S32. For the two-electron oxidized $\mathbf{1Py_2}$ the Soret band is located at 424 nm, and a weak Q-band at 623 nm was also observed. For two-electron oxidized $\mathbf{2Py_2}$ the Soret band is located at 418 nm and the Q-band at 650 nm. The oxidized species seem to be stable over several minutes, but we have not yet studied their stability over a longer period of time, nor did we try to isolate and further characterize them. The lack of observed EPR signal and the broad Soret and weak Q-band suggest that the electronic structure of the two-electron oxidized species can be described either as strongly antiferromagnetically coupled $[\mathbf{Co(IV)L^{\bullet 2-}}]^{2+}$ or as a true singlet $[\mathbf{Co(III)L^-}]^{2+}$ species (L = L1 or L2).

Electronic Structure Calculations. Geometry optimizations using density functional theory were performed using the ORCA package.[46] We chose the PBE0 hybrid functional and def2-SVP basis sets on all atoms, except Co, for which def2-TZVP was used. Single point calculations were performed on the optimized structures using def2-TZVP on all atoms. Further details and references are given in the Supporting Information. The calculations were done on multiple oxidation states of **1** with no, one, or two apical pyridine ligands and for selected oxidized complexes with one pyridine and one hydroxido or oxido ligand. For some species, we added one or more additional H_2O molecules, H-bonded to the apical OH_n species ($n = 0$, 1, or 2). Species with odd number of electrons were calculated as spin-1/2 systems, while for species with even number of electrons, triplet ($S = 1$), true singlet ($S = 0$) and open-shell singlet ($S = 0$ (BS, broken-symmetry)) calculations were performed. Displayed spin densities correspond to the spin states that were found to be the ground state for each species. Broken symmetry calculations were performed using the BrokenSym keyword in ORCA. From spin density plots and observation of the occupation of metal d- and ligand frontier orbitals we could determine the metal and corrole oxidation states for each species. The spin densities for corrole complex **1** with different numbers of bound pyridine ligands and with net charges ranging from −1 to +2 are shown in Figure 7. The species with net charges ranging from −1 to +1 were experimentally identified by EPR, CV, and UV−vis spectroscopy. The two-electron oxidized species were suggested by EPR and UV−vis spectroscopy, but at this point were not confirmed by other analytical means.

The first reduction for the penta-coordinated complex occurs on the metal center, whereas for the hexacoordinated complex, it occurs on the ligand. Calculation of the Gibbs free energies of the different species suggest that the pentacoordinated reduced form $[\mathbf{Co(II)L1^{3-}Py}]^-$ is more stable than the hexacoordinated form $[\mathbf{Co(III)L1^{\bullet 4-}Py_2}]^-$ by about 99 kJ/mol. This computational result is clearly supported by the EPR signal of the reduced corroles.

https://dx.doi.org/10.1021/acs.inorgchem.0c02550
Inorg. Chem. XXXX, XXX, XXX−XXX

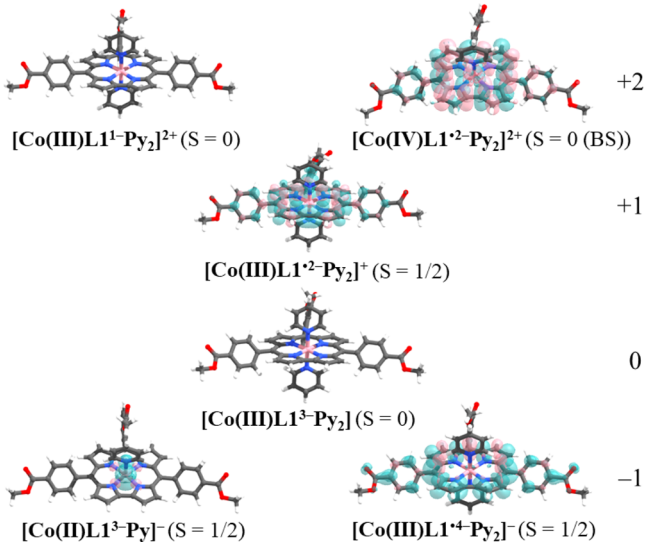

Figure 7. Spin density plots (isovalue = 0.001) of $[\mathbf{1Py}_n]^m$ (n = 1, 2 and m = −1 to +2). The legends indicate the oxidation state of the metal and the charge and radical character of the corrole ligand, as well as the total spin state.

Scheme 3 shows the formulas of the different species of corrole **1** in different oxidation states, together with calculated logarithms of pyridine affinity constants (in red), and redox potentials (in blue), referenced against FcH^+/FcH. The redox potential difference (ΔE) for the first corrole oxidation is quite similar to the experimentally determined value of −0.2 V in DCM, and the ΔE for the first reduction, calculated considering dissociation of one pyridine ligand, is also in reasonable agreement with the experimental value (ΔE_{calcd} = −0.93 V, ΔE_{exp} = −0.77 V). For the second oxidation process the calculated ΔE_{calcd} = 1.08 V value starts to deviate from the experimentally determined ΔE_{exp} = 0.53 V. The reason for this deviation is probably due to the fact that charged species experience stronger solvation effects, and especially counterion pairing in solution, and these effects require a more careful treatment than can be performed using pseudosolvation methods. The log K calculated for binding of pyridine to **Co(III)L1Py** to give **Co(III)L1Py$_2$** is 3.38, which is quite in agreement with the experimentally determined value of 3.68. The good agreement between calculated and experimental values for the neutral forms of the corroles indicate that the proposed structures are probably good descriptions of the real structures of these species in solution, meaning that interactions with the solvent are weak. The calculated affinity constants for pyridine increase with the oxidation state of the corrole. However, for the oxidized and reduced corroles, we do not expect a quantitative prediction of affinity constants or other thermodynamic quantities, as charged species are likely

Scheme 3. Energy Diagram of Cobalt Corrole 1 in Different Oxidation States and Differing Number and Identity of Apical Ligands[a]

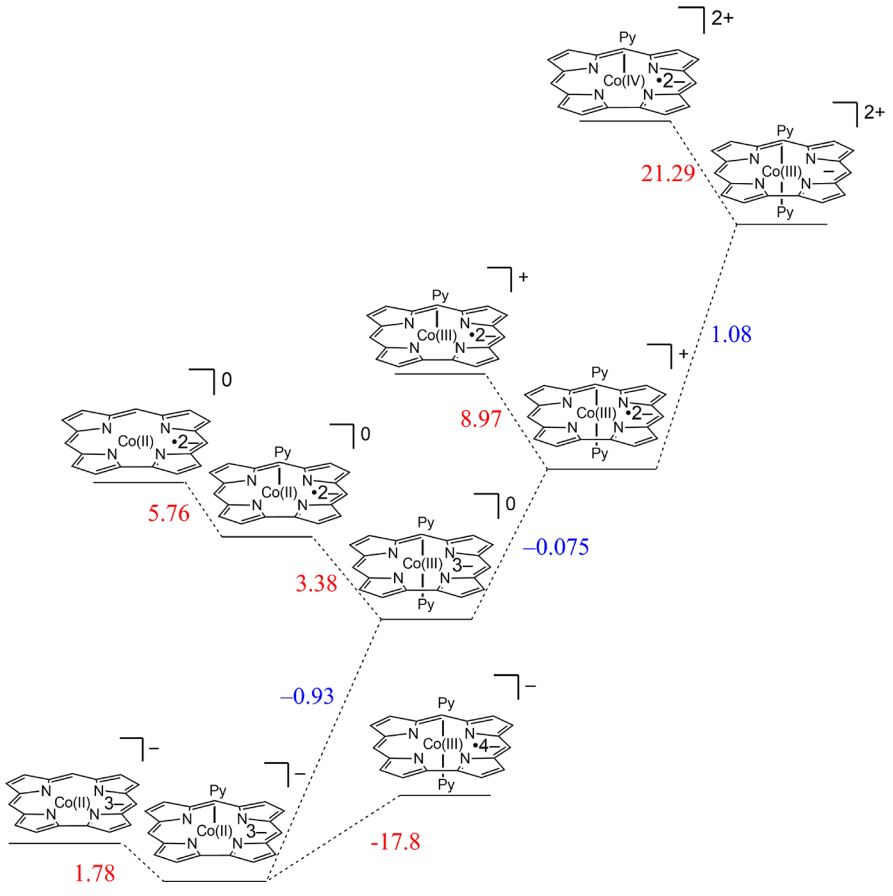

[a]The oxidation states of the Co atom and the corrole according to DFT results are shown. Logarithms of pyridine binding constants are written in red and redox potentials vs. FcH^+/FcH are shown in blue. Calculations were performed using DCM pseudosolvent within the CPCM model.

https://dx.doi.org/10.1021/acs.inorgchem.0c02550
Inorg. Chem. XXXX, XXX, XXX−XXX

to interact more strongly with solvent molecules and counterions.

Electrocatalytic Water Oxidation Studies. The homogeneous electrocatalytic properties of cobalt corroles for water oxidation were studied by means of cyclic voltammetry in MeCN (0.1 M Bu_4NPF_6). Upon addition of increasing amounts of H_2O, $\mathbf{1Py_2}$ and $\mathbf{2Py_2}$ showed catalytic waves coincident with the third corrole oxidation (Figure 8).

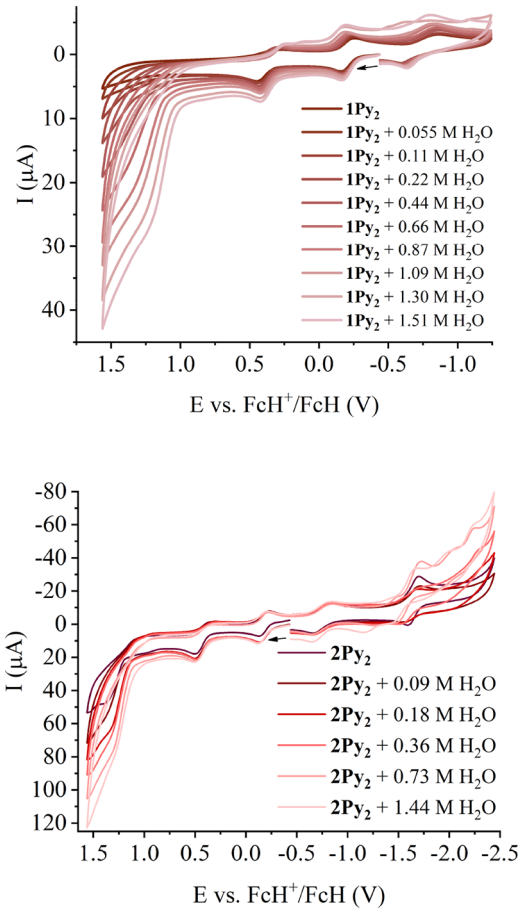

Figure 8. Cyclic voltammetry traces of $\mathbf{1Py_2}$ (top) and $\mathbf{2Py_2}$ (bottom) in MeCN with 0.1 M Bu_4NPF_6 and increasing concentrations of H_2O. Scan rate and direction: 50 mV/s, anodic.

The catalytic waves are slightly shifted to less anodic potentials with increasing amounts of H_2O, reaching peak potentials of 1.225 V for $\mathbf{1Py_2}$ and 1.287 V for $\mathbf{2Py_2}$ with H_2O concentrations of 1.51 and 1.44 M, respectively. The cathodic shift can be explained considering the equilibrium (eq 1)

$$[\mathrm{Co(III)corPy_2}]^{2+} \overset{-e^-}{\underset{+e^-}{\rightleftharpoons}} [\mathrm{Co(III)corPy_2}]^{3+} \overset{+H_2O}{\underset{-Py,H^+}{\rightleftharpoons}} [\mathrm{Co(III)corPy(OH)}]^{2+} \quad (1)$$

where H_2O binding and deprotonation gives an hydroxido (and later oxido) bound species which partially compensates the charge of the triply oxidized corroles. This effect has been discussed by Gross et al.[23] who showed that OH^- and F^- binding caused cathodic shifts of the first and second oxidations of Co(tpfc), although in that case no apical Py ligands were present.

The first corrole oxidation of $\mathbf{1Py_2}$ and $\mathbf{2Py_2}$ remains reversible before and after addition of H_2O, as evidenced by an i_f/i_r (forward/reverse) ratio of 1 (Figure S38 and S39); furthermore, performing several consecutive scans shows no change in the catalytic response. The second oxidation however is partially irreversible which, together with the reversibility of the first oxidation, suggests a competitive equilibrium between H_2O/OH^- and Py, with the former being favored in high oxidation states and the latter in lower oxidation states of the cobalt corrole. The DFT calculated energetics of Py versus H_2O/OH^- coordination for two- and three times oxidized **1** in MeCN pseudosolvent (CPCM) with several explicit H_2O molecules is described in Scheme S2. The calculated redox potential for the third oxidation ($[\mathbf{1Py_2}]^{2+}/[\mathbf{1Py_2}]^{3+}$) is 1.2 V, quite in agreement with the experimental value of 1.26 V in MeCN. Calculations show that the replacement reaction $[\mathbf{1Py_2}]^{2+} \rightarrow [\mathbf{1Py(H_2O)}]^{2+}$ + Py is slightly favored and the reaction $[\mathbf{1Py_2}]^{3+} \rightarrow [\mathbf{1Py(OH)}]^{2+}$ + Py + H^+ even more so. The calculated redox potential for the third oxidation of the aquo ligated cobalt corrole ($[\mathbf{1Py(H_2O)}]^{2+}/[\mathbf{1Py(OH)}]^{2+}$ + H^+) is 0.87 V, which is consistent with the shift of the third oxidation to lower potentials upon increasing H_2O concentration (see Figure S40).

To determine if the observed catalytic current corresponding to H_2O oxidation to O_2, we performed bulk electrolysis experiments in an air-equilibrated cell with $\mathbf{1Py_2}$ in MeCN 0.3 M $LiClO_4$ with 15% H_2O, using a glassy carbon rod with a diameter of 5 mm as working electrode, a Pt wire as counter electrode, and a Ag wire as pseudoreference electrode (see Figures S42 and S43). The current achieved in one experiment was around 500 μA at 1.9 V vs Ag, and it remained approximately constant during several hours, in which a total of 2 mL gas was evolved. After 4 h of electrolysis, a sample of the cell headspace was taken with a gastight syringe and its composition determined with gas chromatography. The headspace gas composition turned out to be 25% O_2 and 75% N_2. This amount of O_2 was consistent with the evolved gas volume of 2 mL, considering that the headspace of the cell plus the bubbler was approximately 17−19 mL. However, given the error of the GC detection method, and the fact that we could only perform one end-point gas analysis, we decided to also perform in situ O_2 gas measurements with a Clark electrode.

For this purpose, we used an FTO-coated glass as the working electrode, as this possesses a much larger surface area than the glassy carbon rod. With this setup, in the same conditions, we were able to achieve currents in the range of 2 mA at 1.95 V vs Ag. Bubbles could be observed slowly forming on the anode and the cathode, the later suggesting H_2 evolution. We performed electrolysis experiments of a solution of $\mathbf{1Py_2}$ in MeCN 0.3 M $LiClO_4$ with 15% H_2O and 2 mM KOH and were able to detect a steady increase in the O_2 concentration in the headspace over 8 h. The plot of the theoretical (based on the faradaic current) and measured amounts of O_2 in the headspace is shown in Figure S44. The average Faradaic efficiency during the first 4 h was 82%. This experiment also demonstrated the ability of $\mathbf{1Py_2}$ to sustain catalysis for at least 8 h. After this time, we stopped O_2 detection but maintained electrolysis 14 more hours, in which the current only decreased slightly.

Having established that the catalytic current for the third oxidation of $\mathbf{1Py_2}$ and $\mathbf{2Py_2}$ corresponds to H_2O oxidation to O_2, we proceeded to calculate the observed catalytic constant

https://dx.doi.org/10.1021/acs.inorgchem.0c02550
Inorg. Chem. XXXX, XXX, XXX−XXX

Table 4. Turnover Frequencies (TOF) and Reported Potentials (E) for Water Oxidation Reactions Catalyzed by Cobalt Corroles and Conditions and Amount of H_2O and Bases

	TOF (s^{-1})	E (V) vs reported reference	E (V) vs FcH^+/FcH	medium	H_2O content	ref
1Py$_2$	1.86		1.29	MeCN, 0.1 M Bu_4NPF_6 (homogeneous)	1.3 M (2.34%)	this work
2Py$_2$	1.67		1.38	MeCN, 0.1 M Bu_4NPF_6 (homogeneous)	1.44 M (2.5%)	this work
Co(tpfc)	0.2	1.4 V vs Ag/AgCl	~0.9	0.1 M KPO_4 buffer, pH 7 (heterogeneous)	solvent	13
	0.77		0.67	MeCN, 0.1 M Bu_4NClO_4, 300 μM TBAOH (homogeneous)	2.66 M (4.8%)	23
Co "Hangman"	0.81	1.4 V vs Ag/AgCl	~0.9	0.1 M KPO_4 buffer, pH 7 (heterogeneous)	solvent	13
Co(BAPC)Py$_2$	0.2	1.4 vs NHE	~0.7	MeCN, 0.1 M Bu_4NPF_6 (homogeneous)	1.7 M (3%)	24

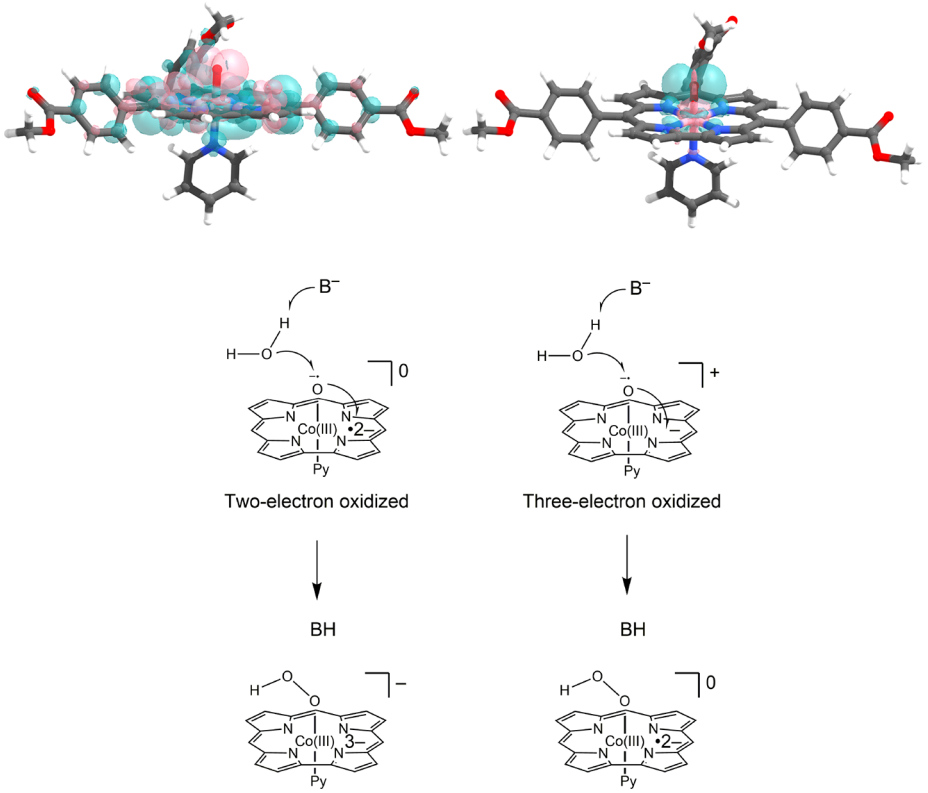

Figure 9. Top panel: Spin density plots of $[\mathbf{Co(III)L1^{\bullet 2-}Py(O^{\bullet -})}]^0$ (left) and $[\mathbf{Co(III)L1^{-}Py(O^{\bullet -})}]^+$ (right). Isovalue = 0.001. Bottom panel: Scheme of the O−O bond formation step by WNA on two-electron-oxidized (left) and three-electron-oxidized (right) cobalt corroles.

k_{obs} for water oxidation, also referred to as turnover frequency (TOF). k_{obs} was calculated from the ratio of the catalytic current i_c of the third oxidation and the peak current i_p of the first oxidation as described in the Supporting Information. The ratios were determined for each H_2O concentration at a scan rate of 50 mV/s. The maximum value obtained for **1Py$_2$** was 1.86 s^{-1} at 1.29 V with 1.30 M H_2O, whereas for **2Py$_2$**, it was 1.67 s^{-1} at 1.38 V with 1.44 M H_2O. Adding larger amounts of H_2O decreased the solubility of both corroles, and the k_{obs} values decreased slightly.

Cobalt corroles containing C_6F_5 groups have been shown to catalyze water oxidation when oxidized twice. For Co(tpfc), a TOF of 0.2 s^{-1} was measured at 1.4 V vs Ag/AgCl (~0.9 V vs FcH^+/FcH).[14] For the cobalt "hangman" corrole, with a pending carboxylate group in a position to abstract H^+ from the attacking H_2O molecule, a TOF of 0.81 s^{-1} was obtained.[13] These experiments were performed by depositing the catalysts on indium tin oxide (ITO) or fluorine-doped tin oxide (FTO) electrodes, and perfoming the electrocatalysis on buffered aqueous media, and therefore are not directly comparable to the experiments performed in this work. However, Gross et al.[23] reported electrocatalytic H_2O oxidation of Co(tpfc) in MeCN with increasing amounts of H_2O and hydroxide in the form of Bu_4NOH. Although in that work the authors did not report the measured TOF, from the reported maximum i_c/i_p ratio of 4 corresponding to the second Co(tpfc) oxidation (Figure 3b in ref 23), and on the basis of their reported scan rate of 0.1 V/s, as well as other experimental conditions, we estimate a TOF of 0.77 s^{-1} at 0.67 V with 2.66 M H_2O and 300 μM TBAOH, which decreases considerably at lower hydroxide concentrations. This shows that for Co(tpfc), the TOFs measured in very different conditions (in $MeCN/H_2O$ homogeneous solution or in aqueous buffer with Co(tpfc) deposited on FTO electrodes) seem to be in reasonable agreement.

https://dx.doi.org/10.1021/acs.inorgchem.0c02550
Inorg. Chem. XXXX, XXX, XXX−XXX

A cobalt corrole with one C_6F_5 and two *p*-aminophenyl substituents (Co(BAPC)Py_2) was also shown to perform water oxidation when oxidized twice, with a k_{obs} of 0.2 s^{-1} at 1.4 V vs NHE, measured in MeCN with 3% (1.7 M) H_2O (~0.7 V vs FcH^+/FcH).[24] We summarize our electrocatalytic findings together with reported data for C_6F_5 containing Co corroles in Table 4.

Our results clearly show that in the case of **1Py$_2$** and **2Py$_2$** the third corrole oxidation is catalytically active for H_2O oxidation, with only a marginal increase in current at the second oxidation process. The k_{obs} values obtained with **1Py$_2$** and **2Py$_2$** are larger than those from previously reported cobalt corroles with C_6F_5 substituents, even with the "hangman" carboxylate, and almost 1 order of magnitude larger than k_{obs} values reported for Co(tpfc) and Co(BAPC)Py_2, in similar conditions.

Additionally, the open-shell nature of our catalytically active species offers the prospect of novel spectroscopic insights into mechanistic details. The mechanism of water oxidation catalyzed by cobalt corroles has been proposed to involve water nucleophilic attack (WNA) on a $[Co(III)L^{\bullet+}(O^{\bullet-})]$ species,[14,47] (Figure 9, lower panel, left). As can be observed in Figure 9 (top panel), the doubly and triply oxidized $[\mathbf{1Py(O)}]^{+/0}$ corroles differ in the charge and spin state of the corrole ligand, but not in the electronic configuration of the cobalt-oxyl moiety (essentially Co(III)-$O^{\bullet-}$). Therefore, it is possible that in both oxidation states the same mechanism for H_2O attack is operative. Doubly oxidized cobalt corrole species possess a total spin of either S = 0 or S = 1, and therefore will be EPR-silent or difficult to observe. On the other hand, our triply oxidized active species would be a spin S = 1/2 system, as would be the immediate product of the attack by H_2O (Figure S9, lower panel, right). Therefore, ideally, some of these species may be detected by EPR; this is not currently possible with Co(tpfc) or *β*-fluorinated Co "hangman" corrole, for which a third oxidation would likely be very hard to achieve.

The potentials at which we obtained the maximum k_{obs} values for **1Py$_2$** and **2Py$_2$** were higher by about 0.3−0.6 V, compared to the potentials at which k_{obs} was reported for Co(tpfc), Co "hangman" corrole and Co(BAPC)Py_2. This is reasonable considering that the latter cobalt corroles displayed electrocatalytic water oxidation activity upon the second oxidation, while **1Py$_2$** and **2Py$_2$** displayed maximum activity upon the third oxidation.

This difference, however, should not be seen as a definitive limitation, as we have observed that the potential of the third oxidation is highly sensitive to the substitution of neutral pyridine by anionic apical ligands, such as hydroxide. Figure S40 shows the change in onset potential for the third oxidation of **2Py$_2$** with increasing H_2O concentration, which shifts from 1.27 V with no H_2O to 1.19 V with 1.44 M H_2O. To qualitatively observe the effect of removing one apical pyridine ligand on the electrocatalytic water oxidation, we performed cyclic voltammetry experiments of **1Py$_2$** in MeCN (0.1 M Bu_4NPF_6) with 2.13 M H_2O before and after adding 0.5 equiv of H_2SO_4 (Figure S41). It can be observed that upon addition of acid there is a large cathodic shift (300 mV) of the third oxidation, and a smaller cathodic shift (130 mV) of the second oxidation of **1Py$_2$**. These changes are consistent with a dissociation of pyridine leading to fast coordination of H_2O, which upon deprotonation lowers the redox potentials of the second and third oxidation. The small amount of acid also shifts the first corrole reduction to higher potentials, which is in agreement with the preference of the reduced Co(II) corrole toward pentacoordination, and consistent with the behavior observed by cyclic voltammetry, EPR, and DFT calculations. As dissociation of pyridine is a requirement for binding of H_2O and achieving maximum catalytic performance, three strategies appear feasible. First, preparing the cobalt corroles **1** and **2** with an apical ligand other than pyridine; one possibility would be DMSO,[48,49] which has been shown to favor pentacoordination. Second, immobilizing the corroles in glassy carbon, graphite, carbon nanotubes,[50] or FTO[22] electrodes and perform heterogeneous water oxidation in aqueous media. Third, performing homogeneous water oxidation studies in aqueous media, for which a water-soluble corrole must be synthesized. A derivative of **1Py$_2$** where the methyl ester groups have been hydrolyzed to the corresponding carboxylic acid groups would seem a suitable target in that respect. We are currently working on some of these leads.

These three strategies require careful characterization of the species involved in electrocatalysis, whether they are corroles **1** and **2** with different apical ligands, adsorbed on electrode surfaces, or a water-soluble analogue of **1**. Furthermore, it is important to compare any new catalytic and mechanistic studies with previously carefully studied systems. The electrochemical, spectroscopic, and computational results obtained in this work provide a solid understanding of the physicochemical properties of cobalt corroles in several oxidations states, which will facilitate the analysis of the behavior of related cobalt corroles during water oxidation catalysis. Particularly, this work has shown that for cobalt corroles with moderately electron-withdrawing groups, the third oxidation is active toward water oxidation, thus opening new alternatives in the mechanistic analysis of this class of catalysts.

In summary, our experimental findings show that using moderate electron withdrawing substituents on cobalt corroles has a profound effect on the catalytic efficiency for water oxidation and point to a triply oxidized cobalt corrole intermediate as active species. In order to confirm or refute this hypothesis, further studies should be performed in which (electro)chemical oxidations coupled to spectroscopic techniques such as EPR, and electronic structure calculations, could play an important role. In this aspect, our careful characterization of the EPR signals associated with several possible species involved in cobalt corrole electrochemistry provide a solid base for identification of certain intermediates in water oxidation catalysis.

4. CONCLUSION

In this work, we have synthesized two cobalt corroles with carboxylic ester and nitro- substituents in their meso-phenyl groups, determined the structure of one of them by single-crystal X-ray diffraction, and studied their (electro)chemical and spectroscopic features by UV−vis and EPR spectroscopy, cyclic voltammetry and spectroelectrochemical methods, as well as density functional theory electronic structure calculations. The synthesized metallocorroles were shown to catalyze water oxidation upon the third corrole oxidation, in contrast with previously reported C_6F_5-containing cobalt corroles, for which the second oxidation has been shown to be active. The obtained TOF value for **1Py$_2$** was 1.86 s^{-1} at 1.29 V with 1.30 M H_2O, whereas for **2Py$_2$** it was 1.67 s^{-1} at 1.38 V with 1.44 M H_2O. These values are larger than for previously reported cobalt corroles with pentafluorophenyl

https://dx.doi.org/10.1021/acs.inorgchem.0c02550
Inorg. Chem. XXXX, XXX, XXX−XXX

substituents, likely because of the extra charge in the corrole macrocycle, accessible because of the lower redox potentials of $\mathbf{1Py_2}$ and $\mathbf{2Py_2}$. The higher catalytic turnover frequency comes at the expense of a larger overpotential.

Our findings encourage subsequent studies of water oxidation catalysis employing cobalt corroles with electron-donating groups and highlight the importance of tuning of the substituents on the corrole moiety for optimizing catalytic behavior of the corresponding metal complexes.

■ ASSOCIATED CONTENT

Supporting Information

The Supporting Information is available free of charge at https://pubs.acs.org/doi/10.1021/acs.inorgchem.0c02550.

Experimental details and analytical data of the synthesized complexes; further spectroscopic (UV−visible−NIR, EPR spectroscopy), crystallographic, cyclic voltammetric, and water oxidation electrocatalytic results; details on electronic structure calculations and molecular coordinates from DFT optimizations (PDF)

Accession Codes

CCDC 1915356 contains the supplementary crystallographic data for this paper. These data can be obtained free of charge via www.ccdc.cam.ac.uk/structures, or by emailing data_request@ccdc.cam.ac.uk, or by contacting The Cambridge Crystallographic Data Centre, 12 Union Road, Cambridge CB2 1EZ, UK; fax: + 44 1223 336033.

■ AUTHOR INFORMATION

Corresponding Authors

Nicolás I. Neuman − *Institut für Chemie und Biochemie, Anorganische Chemie, Freie Universität Berlin, Berlin 14195, Germany; Instituto de Desarrollo Tecnológico para la Industria Química, INTEC, UNL-CONICET Paraje El Pozo, Santa Fe, Argentina; Institut für Anorganische Chemie, Universität Stuttgart, Stuttgart D-70569, Germany;* orcid.org/0000-0003-3368-0228; Email: nneuman@intec.unl.edu.ar

Biprajit Sarkar − *Institut für Chemie und Biochemie, Anorganische Chemie, Freie Universität Berlin, Berlin 14195, Germany; Lehrstuhl für Anorganische Koordinationschemie, Institut für Anorganische Chemie, Universität Göttingen, Göttingen 37077, Germany;* orcid.org/0000-0003-4887-7277; Email: biprajit.sarkar@iac.uni-stuttgart.de

Authors

Uta Albold − *Institut für Chemie und Biochemie, Anorganische Chemie, Freie Universität Berlin, Berlin 14195, Germany*

Eleonora Ferretti − *Institut für Chemie und Biochemie, Anorganische Chemie, Freie Universität Berlin, Berlin 14195, Germany;* orcid.org/0000-0002-8918-3880

Shubhadeep Chandra − *Institut für Chemie und Biochemie, Anorganische Chemie, Freie Universität Berlin, Berlin 14195, Germany*

Simon Steinhauer − *Institut für Chemie und Biochemie, Anorganische Chemie, Freie Universität Berlin, Berlin 14195, Germany;* orcid.org/0000-0001-7420-1153

Paul Rößner − *Institut für Technische Chemie, Universität Stuttgart, Stuttgart D-70569, Germany*

Franc Meyer − *Institut für Anorganische Chemie, Universität Göttingen, Göttingen 37077, Germany;* orcid.org/0000-0002-8613-7862

Fabio Doctorovich − *Departamento de Química Inorgánica; Analítica y Química Física/INQUIMAE-CONICET; Facultad de Ciencias Exactas y Naturales, Universidad de Buenos Aires, Ciudad Universitaria, Pabellón II, Buenos Aires C1428EHA, Argentina;* orcid.org/0000-0003-1088-2089

Santiago E. Vaillard − *Instituto de Desarrollo Tecnológico para la Industria Química, INTEC, UNL-CONICET Paraje El Pozo, Santa Fe, Argentina;* orcid.org/0000-0002-7863-3348

Complete contact information is available at: https://pubs.acs.org/10.1021/acs.inorgchem.0c02550

Notes

The authors declare no competing financial interest.

■ ACKNOWLEDGMENTS

This work was possible because of funds provided by ANPCyT (PICT 2015 N° 0101), CONICET, and the Alexander von Humboldt Foundation (Postdoctoral stipend to N.I.N.). N.I.N., S.E.V., and F.D. are members of CONICET. We thank Prof. Dr. Elias Klemm for providing us access to GC equipment. We thank Simon Suhr for useful discussions. The core facility (BioSupraMol) of the FU Berlin is gratefully acknowledged. The present work made use of computational resources of the Pirayu cluster, acquired with funds of the Agencia Santafesina de Ciencia, Tecnología e Innovación (ASACTEI), Gobierno de la Provincia de Santa Fe, through the project AC-00010-18, Resolution No 117/14. This equipment is part of the Sistema Nacional de Computación de Alto Desempeño of the Ministerio de Ciencia y Tecnología de la República Argentina. Additionally, the computational facility of the ZEDAT, FU Berlin, is acknowledged.

■ DEDICATION

Dedicated to Prof. Peter Klüfers on the occassion of his 70th birthday.

■ REFERENCES

(1) Aviv, I.; Gross, Z. Corrole-based applications. *Chem. Commun.* **2007**, No. 20, 1987−1999.

(2) Aviv-Harel, I.; Gross, Z. Aura of corroles. *Chem. - Eur. J.* **2009**, *15* (34), 8382−8394.

(3) Fang, Y.; Ou, Z.; Kadish, K. M. Electrochemistry of Corroles in Nonaqueous Media. *Chem. Rev.* **2017**, *117* (4), 3377−3419.

(4) Ghosh, A. Electronic Structure of Corrole Derivatives: Insights from Molecular Structures, Spectroscopy, Electrochemistry, and Quantum Chemical Calculations. *Chem. Rev.* **2017**, *117* (4), 3798−3881.

(5) Gonglach, S.; Paul, S.; Haas, M.; Pillwein, F.; Sreejith, S. S.; Barman, S.; De, R.; Müllegger, S.; Gerschel, P.; Apfel, U.-P.; Coskun, H.; Aljabour, A.; Stadler, P.; Schöfberger, W.; Roy, S. Molecular cobalt corrole complex for the heterogeneous electrocatalytic reduction of carbon dioxide. *Nat. Commun.* **2019**, *10* (1), 3864.

(6) Gross, Z.; Simkhovich, L.; Galili, N. First catalysis by corrole metal complexes: epoxidation, hydroxylation, and cyclopropanation. *Chem. Commun.* **1999**, No. 7, 599−600.

(7) Mondal, B.; Sengupta, K.; Rana, A.; Mahammed, A.; Botoshansky, M.; Dey, S. G.; Gross, Z.; Dey, A. Cobalt corrole catalyst for efficient hydrogen evolution reaction from H2O under ambient conditions: reactivity, spectroscopy, and density functional theory calculations. *Inorg. Chem.* **2013**, *52* (6), 3381−3387.

(8) Mahammed, A.; Mondal, B.; Rana, A.; Dey, A.; Gross, Z. The cobalt corrole catalyzed hydrogen evolution reaction: surprising

https://dx.doi.org/10.1021/acs.inorgchem.0c02550
Inorg. Chem. XXXX, XXX, XXX−XXX

electronic effects and characterization of key reaction intermediates. *Chem. Commun.* **2014**, *50* (21), 2725−2727.
(9) Morales Vásquez, M. A.; Hamer, M.; Neuman, N. I.; Tesio, A. Y.; Hunt, A.; Bogo, H.; Calvo, E. J.; Doctorovich, F. Iron and Cobalt Corroles in Solution and on Carbon Nanotubes as Molecular Photocatalysts for Hydrogen Production by Water Reduction. *ChemCatChem* **2017**, *9* (16), 3259−3268.
(10) Kadish, K. M.; Frémond, L.; Ou, Z.; Shao, J.; Shi, C.; Anson, F. C.; Burdet, F.; Gros, C. P.; Barbe, J.-M.; Guilard, R. Cobalt(III) corroles as electrocatalysts for the reduction of dioxygen: reactivity of a monocorrole, biscorroles, and porphyrin-corrole dyads. *J. Am. Chem. Soc.* **2005**, *127* (15), 5625−5631.
(11) Schechter, A.; Stanevsky, M.; Mahammed, A.; Gross, Z. Four-electron oxygen reduction by brominated cobalt corrole. *Inorg. Chem.* **2012**, *51* (1), 22−24.
(12) Grodkowski, J.; Neta, P.; Fujita, E.; Mahammed, A.; Simkhovich, L.; Gross, Z. Reduction of Cobalt and Iron Corroles and Catalyzed Reduction of CO_2. *J. Phys. Chem. A* **2002**, *106* (18), 4772−4778.
(13) Dogutan, D. K.; McGuire, R.; Nocera, D. G. Electocatalytic water oxidation by cobalt(III) hangman β-octafluoro corroles. *J. Am. Chem. Soc.* **2011**, *133* (24), 9178−9180.
(14) Lei, H.; Han, A.; Li, F.; Zhang, M.; Han, Y.; Du, P.; Lai, W.; Cao, R. Electrochemical, spectroscopic and theoretical studies of a simple bifunctional cobalt corrole catalyst for oxygen evolution and hydrogen production. *Phys. Chem. Chem. Phys.* **2014**, *16* (5), 1883−1893.
(15) Dau, H.; Limberg, C.; Reier, T.; Risch, M.; Roggan, S.; Strasser, P. The Mechanism of Water Oxidation: From Electrolysis via Homogeneous to Biological Catalysis. *ChemCatChem* **2010**, *2* (7), 724−761.
(16) Matheu, R.; Garrido-Barros, P.; Gil-Sepulcre, M.; Ertem, M. Z.; Sala, X.; Gimbert-Suriñach, C.; Llobet, A. The development of molecular water oxidation catalysts. *Nat. Rev. Chem.* **2019**, *3* (5), 331−341.
(17) Blakemore, J. D.; Crabtree, R. H.; Brudvig, G. W. Molecular Catalysts for Water Oxidation. *Chem. Rev.* **2015**, *115* (23), 12974−13005.
(18) Hunter, B. M.; Gray, H. B.; Müller, A. M. Earth-Abundant Heterogeneous Water Oxidation Catalysts. *Chem. Rev.* **2016**, *116* (22), 14120−14136.
(19) Fukuzumi, S.; Hong, D. Homogeneous versus Heterogeneous Catalysts in Water Oxidation. *Eur. J. Inorg. Chem.* **2014**, *2014* (4), 645−659.
(20) Gao, Y.; Akermark, T.; Liu, J.; Sun, L.; Akermark, B. Nucleophilic attack of hydroxide on a Mn(V) oxo complex: a model of the O-O bond formation in the oxygen evolving complex of photosystem II. *J. Am. Chem. Soc.* **2009**, *131* (25), 8726−8727.
(21) Simkhovich, L.; Galili, N.; Saltsman, I.; Goldberg, I.; Gross, Z. Coordination chemistry of the novel 5,10,15-tris(pentafluorophenyl)-corrole: synthesis, spectroscopy, and structural characterization of its cobalt(III), rhodium(III), and iron(IV) complexes. *Inorg. Chem.* **2000**, *39* (13), 2704−2705.
(22) Xu, L.; Lei, H.; Zhang, Z.; Yao, Z.; Li, J.; Yu, Z.; Cao, R. The effect of the trans axial ligand of cobalt corroles on water oxidation activity in neutral aqueous solutions. *Phys. Chem. Chem. Phys.* **2017**, *19* (15), 9755−9761.
(23) Sinha, W.; Mizrahi, A.; Mahammed, A.; Tumanskii, B.; Gross, Z. Reactive Intermediates Involved in Cobalt Corrole Catalyzed Water Oxidation (and Oxygen Reduction). *Inorg. Chem.* **2018**, *57* (1), 478−485.
(24) Kumar, A.; Sujesh, S.; Varshney, P.; Paul, A.; Jeyaraman, S. Aminophenyl-substituted cobalt(iii) corrole: a bifunctional electro-catalyst for the oxygen and hydrogen evolution reactions. *Dalton Trans.* **2019**, *48* (30), 11345−11351.
(25) Gross, Z.; Galili, N.; Saltsman, I. The First Direct Synthesis of Corroles from Pyrrole. *Angew. Chem., Int. Ed.* **1999**, *38* (10), 1427−1429.
(26) Paolesse, R.; Mini, S.; Sagone, F.; Boschi, T.; Jaquinod, L.; Nurco, D. J.; Smith, K. M. 5,10,15-Triphenylcorrole: a product from a modified Rothemund reaction. *Chem. Commun.* **1999**, No. 14, 1307−1308.
(27) Harmer, J.; van Doorslaer, S.; Gromov, I.; Bröring, M.; Jeschke, G.; Schweiger, A. A Pulse EPR and ENDOR Investigation of the Electronic Structure of a σ-Carbon-Bonded Cobalt(IV) Corrole. *J. Phys. Chem. B* **2002**, *106* (10), 2801−2811.
(28) Li, B.; Ou, Z.; Meng, D.; Tang, J.; Fang, Y.; Liu, R.; Kadish, K. M. Cobalt triarylcorroles containing one, two or three nitro groups. Effect of NO_2 substitution on electrochemical properties and catalytic activity for reduction of molecular oxygen in acid media. *J. Inorg. Biochem.* **2014**, *136*, 130−139.
(29) Gao, Y.; Liu, J.; Wang, M.; Na, Y.; Åkermark, B.; Sun, L. Synthesis and characterization of manganese and copper corrole xanthene complexes as catalysts for water oxidation. *Tetrahedron* **2007**, *63* (9), 1987−1994.
(30) Sinha, W.; Mahammed, A.; Fridman, N.; Gross, Z. Water Oxidation Catalysis by Mono- and Binuclear Iron Corroles. *ACS Catal.* **2020**, *10* (6), 3764−3772.
(31) Koszarna, B.; Gryko, D. T. Efficient synthesis of meso-substituted corroles in a H2O-MeOH mixture. *J. Org. Chem.* **2006**, *71* (10), 3707−3717.
(32) Ganguly, S.; Conradie, J.; Bendix, J.; Gagnon, K. J.; McCormick, L. J.; Ghosh, A. Electronic Structure of Cobalt-Corrole-Pyridine Complexes: Noninnocent Five-Coordinate Co(II) Corrole-Radical States. *J. Phys. Chem. A* **2017**, *121* (50), 9589−9598.
(33) Guilard, R.; Gros, C. P.; Bolze, F.; Jérôme, F.; Ou, Z.; Shao, J.; Fischer, J.; Weiss, R.; Kadish, K. M. Alkyl and Aryl Substituted Corroles. 1. Synthesis and Characterization of Free Base and Cobalt Containing Derivatives. X-ray Structure of $(Me_4Ph_5Cor)Co(py)_2$. *Inorg. Chem.* **2001**, *40* (19), 4845−4855.
(34) Jiang, X.; Naitana, M. L.; Desbois, N.; Quesneau, V.; Brandès, S.; Rousselin, Y.; Shan, W.; Osterloh, W. R.; Blondeau-Patissier, V.; Gros, C. P.; Kadish, K. M. Electrochemistry of Bis(pyridine)cobalt (Nitrophenyl)corroles in Nonaqueous Media. *Inorg. Chem.* **2018**, *57* (3), 1226−1241.
(35) Kadish, K. M.; Shen, J.; Frémond, L.; Chen, P.; El Ojaimi, M.; Chkounda, M.; Gros, C. P.; Barbe, J.-M.; Ohkubo, K.; Fukuzumi, S.; Guilard, R. Clarification of the oxidation state of cobalt corroles in heterogeneous and homogeneous catalytic reduction of dioxygen. *Inorg. Chem.* **2008**, *47* (15), 6726−6737.
(36) van der Meer, M.; Rechkemmer, Y.; Peremykin, I.; Hohloch, S.; van Slageren, J.; Sarkar, B. (Electro)catalytic C-C bond formation reaction with a redox-active cobalt complex. *Chem. Commun.* **2014**, *50* (76), 11104−11106.
(37) Fritsch, J. M.; McNeill, K. Aqueous reductive dechlorination of chlorinated ethylenes with tetrakis(4-carboxyphenyl)porphyrin cobalt. *Inorg. Chem.* **2005**, *44* (13), 4852−4861.
(38) Dogutan, D. K.; Stoian, S. A.; McGuire, R.; Schwalbe, M.; Teets, T. S.; Nocera, D. G. Hangman corroles: efficient synthesis and oxygen reaction chemistry. *J. Am. Chem. Soc.* **2011**, *133* (1), 131−140.
(39) Aranzaes, J. R.; Daniel, M.-C.; Astruc, D. Metallocenes as references for the determination of redox potentials by cyclic voltammetry - Permethylated iron and cobalt sandwich complexes, inhibition by polyamine dendrimers, and the role of hydroxy-containing ferrocenes. *Can. J. Chem.* **2006**, *84* (2), 288−299.
(40) Krejčik, M.; Daněk, M.; Hartl, F. Simple construction of an infrared optically transparent thin-layer electrochemical cell: Applications to the redox reactions of ferrocene, $Mn_2(CO)_{10}$ and $Mn(CO)_3$(3,5-di-t-butyl-catecholate)$^-$. *J. Electroanal. Chem. Interfacial Electrochem.* **1991**, *317* (1), 179−187.
(41) Stoll, S.; Schweiger, A. Easy Spin, a comprehensive software package for spectral simulation and analysis in EPR. *J. Magn. Reson.* **2006**, *178* (1), 42−55.
(42) Mittra, K.; Mondal, B.; Mahammed, A.; Gross, Z.; Dey, A. Dioxygen bound cobalt corroles. *Chem. Commun.* **2017**, *53* (5), 877−880.

https://dx.doi.org/10.1021/acs.inorgchem.0c02550
Inorg. Chem. XXXX, XXX, XXX−XXX

(43) Walker, F. A. Electron spin resonance study of coordination to the fifth and sixth positions of.alpha.,.beta.,.gamma.,.delta.-tetra(p-methoxyphenyl)porphinatocobalt(II). *J. Am. Chem. Soc.* **1970**, *92* (14), 4235−4244.
(44) Ramdhanie, B.; Telser, J.; Caneschi, A.; Zakharov, L. N.; Rheingold, A. L.; Goldberg, D. P. An example of O2 binding in a cobalt(II) corrole system and high-valent cobalt-cyano and cobalt-alkynyl complexes. *J. Am. Chem. Soc.* **2004**, *126* (8), 2515−2525.
(45) Connelly, N. G.; Geiger, W. E. Chemical Redox Agents for Organometallic Chemistry. *Chem. Rev.* **1996**, *96* (2), 877−910.
(46) Neese, F. Software update: the ORCA program system, version 4.0. *Wiley Interdiscip. Rev.: Comput. Mol. Sci.* **2018**, *8* (1), No. e1327.
(47) Lai, W.; Cao, R.; Dong, G.; Shaik, S.; Yao, J.; Chen, H. Why Is Cobalt the Best Transition Metal in Transition-Metal Hangman Corroles for O-O Bond Formation during Water Oxidation? *J. Phys. Chem. Lett.* **2012**, *3* (17), 2315−2319.
(48) Jiang, X.; Shan, W.; Desbois, N.; Quesneau, V.; Brandès, S.; van Caemelbecke, E.; Osterloh, W. R.; Blondeau-Patissier, V.; Gros, C. P.; Kadish, K. M. Mono-DMSO ligated cobalt nitrophenylcorroles: electrochemical and spectral characterization. *New J. Chem.* **2018**, *42* (10), 8220−8229.
(49) Osterloh, W. R.; Quesneau, V.; Desbois, N.; Brandès, S.; Shan, W.; Blondeau-Patissier, V.; Paolesse, R.; Gros, C. P.; Kadish, K. M. Synthesis and the Effect of Anions on the Spectroscopy and Electrochemistry of Mono(dimethyl sulfoxide)-Ligated Cobalt Corroles. *Inorg. Chem.* **2020**, *59* (1), 595−611.
(50) Lei, H.; Liu, C.; Wang, Z.; Zhang, Z.; Zhang, M.; Chang, X.; Zhang, W.; Cao, R. Noncovalent immobilization of a pyrene-modified cobalt corrole on carbon supports for enhanced electrocatalytic oxygen reduction and oxygen evolution in aqueous solutions. *ACS Catal.* **2016**, *6* (10), 6429−6437.

https://dx.doi.org/10.1021/acs.inorgchem.0c02550
Inorg. Chem. XXXX, XXX, XXX−XXX